

Study on Slag Phase Erosion Behavior and Mechanism of Carbon Composite Brick in Hydrogen-Rich Blast Furnace Hearth



Mingbo Song, Kexin Jiao, Cui Wang, Jianliang Zhang, and Chuan Wang

Abstract In this study, through thermodynamic calculation, the possible reactions of carbon composite bricks in a high-temperature water vapor environment were analyzed. The morphology of carbon composite bricks after water vapor erosion was investigated through a water vapor oxidation experiment. In addition, a damage investigation was carried out on a blast furnace using hydrogen-rich gas smelting. During the period, a green-white phase with a thickness of 150 mm–200 mm was found inside the carbon composite brick in the taphole area. The carbon bricks in this area were sampled, and XRD, chemical analysis, and SEM–EDS detection were carried out. The test results show that there is blast furnace slag erosion and harmful element Zn erosion in carbon composite bricks. The erosion of harmful elements caused the expansion and ring cracking of carbon composite bricks, resulting in further slag erosion, which eventually led to the macroscopic slag phase erosion in the taphole area. The service life of carbon composite bricks can be effectively improved by optimizing the structure of carbon composite bricks, reducing the number of pores, optimizing the pore structure, and promoting the formation of a slag-rich protective layer on the hot surface of carbon composite bricks by improving the structure of blast furnace slag system.

Keywords Hydrogen-rich blast furnace · Carbon composite bricks · Slag phase erosion · Ring crack expansion

M. Song · K. Jiao (✉) · C. Wang · J. Zhang · C. Wang
School of Metallurgical and Ecological Engineering, University of Science and Technology
Beijing, Beijing 100083, China
e-mail: jiaokexin_ustb@126.com

J. Zhang · C. Wang
School of Chemical Engineering, The University of Queensland, St Lucia, QLD 4072, Australia

Introduction

Under the condition of global carbon neutrality, reducing carbon emissions has become a new trend in the development of the steel industry [1–3]. The blast furnace is the largest vertical reactor, which currently bears the vast majority of the current hot metal production work [4]. In the normal production process, the blast furnace hearth is full of high-temperature slag iron, so the blast furnace hearth becomes the limiting link of the blast furnace life. In recent years, with the continuous improvement of blast furnace smelting strength, accidents of blast furnace hearth burning have occurred from time to time, which also makes blast furnace workers pay more attention to the research of blast furnace hearth refractory [5–9].

Zuo et al. studied the dissolution of Al_2O_3 and SiO_2 in carbon composite bricks through blast furnace slag erosion experiments, which is the main reason for the erosion of carbon composite bricks during use [10]. Therefore, slag corrosion resistance has become an important performance of refractory materials in the hearth [11]. Through static and dynamic erosion experiments, the researchers studied the high-temperature slag-iron erosion, chemical erosion behavior, and thermal stress erosion of hearth carbon bricks under different atmospheres [12–15]. However, there are few studies on the erosion behavior of hearth refractory in a water vapor environment. In the context of hydrogen-rich smelting, the research on the erosion phenomenon and erosion mechanism of carbon composite bricks in the hearth area is not sufficient [16, 17].

With the help of blast furnace damage investigation, the erosion of the hearth refractory after service can be studied intuitively. In this study, the erosion behavior of carbon composite bricks after service was studied through damage investigation and sampling of refractory materials in the hearth area of a hydrogen-rich blast furnace. The water vapor erosion experiment in the laboratory stage studied the erosion phenomenon of carbon composite bricks under the action of water vapor, and the erosion mechanism of carbon composite bricks under the condition of hydrogen-rich smelting was clarified.

Experimental

Experimental Apparatus and Samples

Through cutting, grinding, and polishing, the sample is made into a sheet sample with a specification of $\text{Ø}\phi 12 \times 5$ mm, as shown in Fig. 1.

The experiment uses a single variable method. When a certain component is changed, other factors remain unchanged. The schematic diagram of the experimental device is shown in Fig. 2.

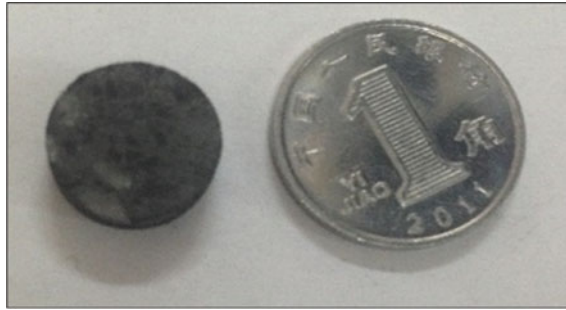


Fig. 1 Morphology of carbon composite brick sample

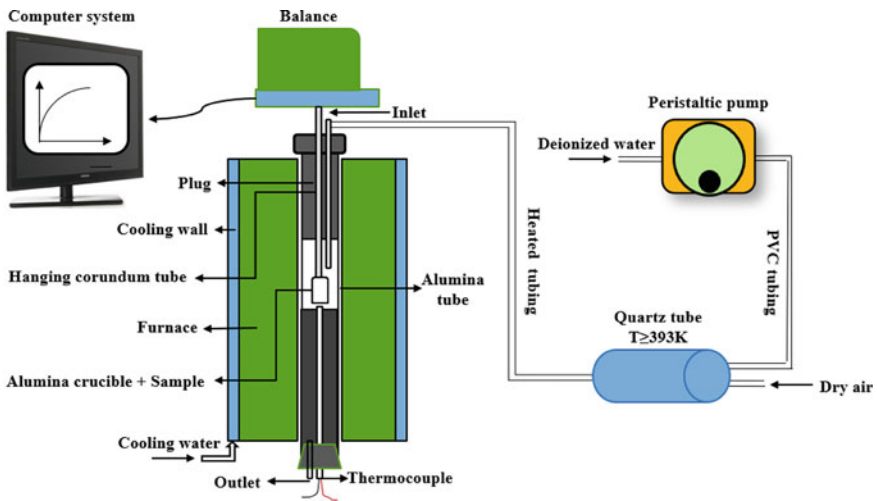


Fig. 2 Schematic diagram of high-temperature water vapor thermogravimetric device

- (1) Heating and sample preparation: Run the high-temperature tube furnace, open the FP-93 temperature control instrument, set the heating program (group number, segment number, etc.), and heat the high-temperature furnace to the specified temperature; at the same time, prepare samples and weigh them.
- (2) Set the reaction atmosphere: Open the XMTD temperature control instrument, adjust the temperature of the mixing tank to 300 °C; open the XMTG digital display regulator, and adjust the temperature of the heating line to 100 °C. Open the gas cylinder and adjust the gas flow; when the above two temperatures reach the specified value, the injection pump is opened and the continuous mode operation is adopted to adjust the water vapor flow and run, and the ventilation is about 30 min in advance.
- (3) Software operation: Open the balance, open the preheating 30 min in advance and the computer switch, open the computer reading window, click on 'open the

serial port', set the data preservation path, and detect whether the connection is successful.

- (4) Lofting and counting: Put the sample into the reaction furnace, insert the quartz tube to ventilate, and click on 'clear the buffer' to start the measurement.
- (5) End of the operation: Click 'close the serial port' and 'save the data', take out the sample, turn off the water vapor generating device (pay attention to the jet pump, turn off XMTD and XMTG after 10 min, turn off the gas flowmeter when the indication is reduced to room temperature, turn off the gas), and turn off the balance.

Experimental Scheme

The experimental schemes at different temperatures are shown in Table 1. The water vapor content is 20%, and the volume flow rate is calculated as follows:

The volume flow rate of carrier gas (air or argon, taking air as an example) is 200 ml/min.

$$w_{\text{H}_2\text{O}(g)} = 20\% = \frac{V_{\text{H}_2\text{O}(g)}}{V_{\text{H}_2\text{O}(g)} + V_{\text{air}}} \times 100\%, \quad V_{\text{H}_2\text{O}(g)} = 50 \text{ ml/min}$$

Because the liquid water density at 4 °C is $\rho_{\text{H}_2\text{O}(l)} = 1.0 \times 10^3 \text{ kg/m}^3$.

The density of water vapor at 100 °C = 0.6 kg/m^3 .

According to the gas isothermal equation:

$$V_{\text{H}_2\text{O}(l)} = \frac{\rho_{\text{H}_2\text{O}(g)} V_{\text{H}_2\text{O}(g)}}{\rho_{\text{H}_2\text{O}(l)}} = \frac{0.6 \times 50}{1.0 \times 10^3} = 0.03 \text{ ml/min}.$$

The volume flow rate was 1.8 ml/h.

Table 1 Experimental scheme of oxidation resistance of refractory at different temperatures

Peer group	Brick type	Temperature/°C	Atmosphere
1	Carbon composite bricks	800	Air (200 ml) + 20% H ₂ O (1.8 ml/h)
2	Carbon composite bricks	1000	Air (200 ml) + 20% H ₂ O (1.8 ml/h)
3	Carbon composite bricks	1200	Air (200 ml) + 20% H ₂ O (1.8 ml/h)

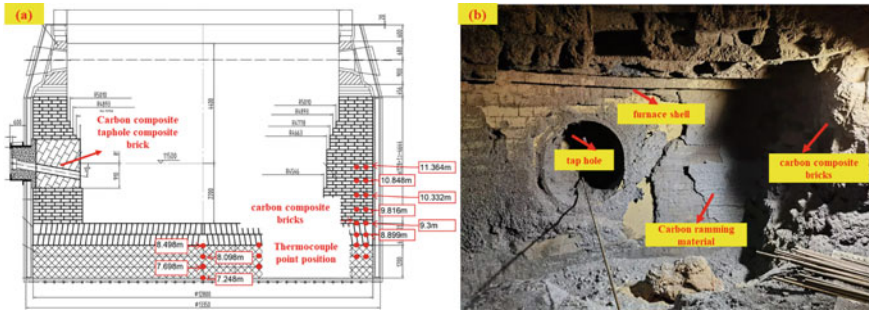


Fig. 3 Blast furnace hearth refractory configuration and sampling position with **a** blast furnace hearth refractory configuration and **b** macroscopic morphology of sampling position in taphole area

Sample Preparation After Service

The sample was taken from an 1860 m³ hydrogen-rich blast furnace with 26 tuyeres and 2 tap holes. The refractory configuration of the hearth area and the size of the hearth area are shown in Fig. 3. It can be seen that the side wall of the hearth adopts the refractory configuration of small carbon composite bricks, and the hot surface of the bottom of the furnace is laid with two layers of large carbon composite bricks. The taphole adopts the combination of cold surface integral pouring technology and hot surface carbon composite taphole composite brick.

Analysis and Detection Methods

XRD was used to analyze the phase of the original brick sample of carbon composite brick. The Gibbs free energy of the possible reaction between the water vapor and carbon brick phase was calculated by FactSage. SEM–EDS was used to observe the microstructure of the sample and analyze the elemental composition.

Results and Discussion

Thermomechanical Analysis

Figure 4 shows the X-ray diffraction (XRD) patterns of carbon composite bricks. The main components of carbon composite bricks are C, SiO₂, Al₂O₃, and SiC, and the mass fractions of C, Si, and Al are 10.70%, 7.17%, and 36.62%, respectively.

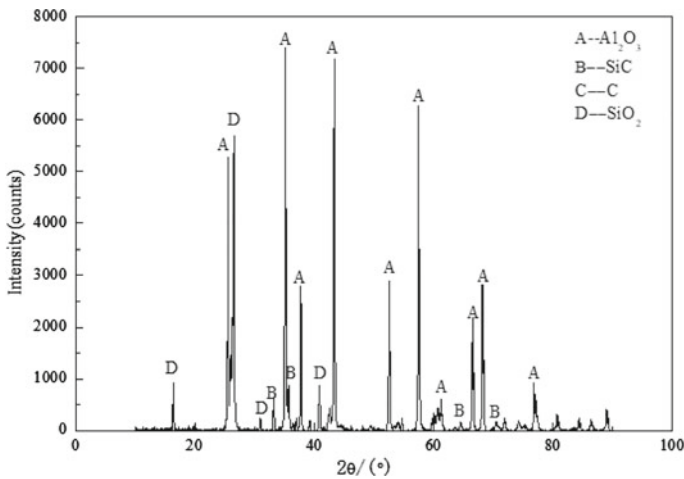
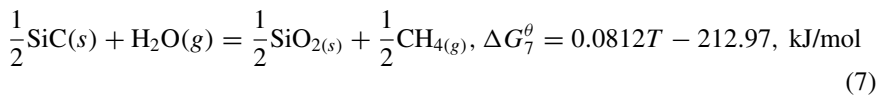
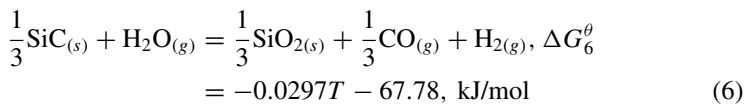
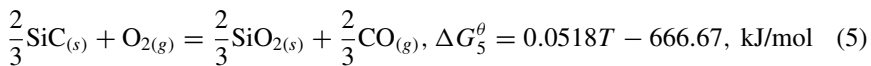
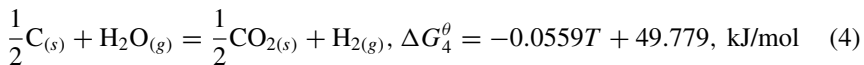
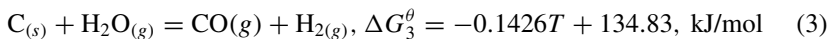
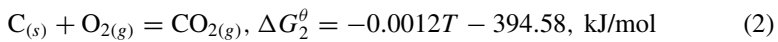
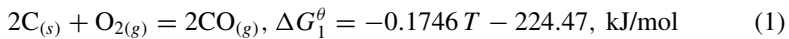


Fig. 4 XRD patterns of carbon composite bricks

The oxidation process of carbon composite bricks under wet air, dry air, and wet argon conditions is mainly that graphite C or SiC reacts with oxygen in water vapor or air to form CO or CO₂ and H₂. The equation of the specific reaction and the Gibbs free energy can be seen as shown in Fig. 5:



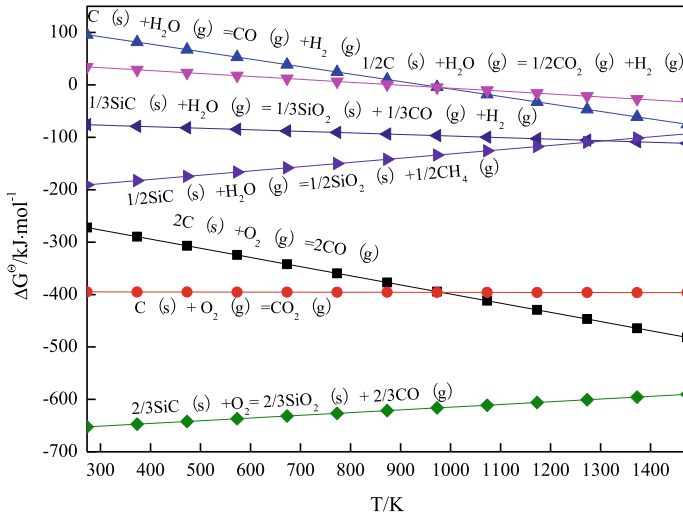


Fig. 5 Gibbs curve of refractory in different atmospheres

- (1) The reaction of refractories in the air and water vapor atmosphere is negative at high temperatures (above 1000 K: this is the lowest temperature of refractory working environment in hydrogen-rich smelting blast furnace hearth), indicating that the reaction can be carried out from the thermodynamic point of view under the experimental temperature conditions.
- (2) The reaction of graphite C, SiC, and O_2 can be carried out at 800 °C, and the reaction of SiC and water vapor can be carried out at 800 °C.
- (3) The reaction of graphite C with O_2 and water vapor decreases with the increase in temperature, indicating that the oxidation reaction of graphite C is endothermic, and the higher the temperature, the easier the reaction.
- (4) The reaction between SiC and O_2 increases with the increase in temperature, indicating that the oxidation reaction of SiC is exothermic. The higher the temperature, the more unfavorable the reaction between SiC and O_2 .
- (5) The reaction of SiC with water vapor to generate CH_4 increases with the increase in temperature, indicating that the reaction is exothermic, and the higher the temperature, the more difficult it is to carry out. The reaction of SiC with water vapor to generate CO decreases with the increase in temperature, indicating that the reaction is endothermic, and the higher the temperature, the easier the reaction is to carry out.

In summary, under the experimental conditions, graphite C and SiC in carbon composite bricks can be oxidized under air and water vapor conditions.

Analysis of Experimental Results of Water Vapor Erosion

Figure 6 shows the weight loss curve of carbon composite brick under different temperatures and wet air conditions. It can be seen from the diagram that in the temperature range of 800–1200 °C, the weight loss rate at 800 °C is the slowest, while the weight loss rate at 1000 °C and 1200 °C is similar. It can be seen from the kinetic curve that the reaction rate at 1200 °C was faster than 1000 °C at the beginning of the reaction, and the two almost coincided in the later period. The time for the three to reach the maximum weight loss rate was 2.5 h, 2 h, and 2 h, respectively.

Figure 7 shows the scanning electron microscope (SEM) images of the reaction cross section of carbon composite bricks after reaction at 800, 1000, and 1200 °C under humid air conditions. The surface of carbon composite bricks is the most rough at 1000 °C, indicating a high degree of oxidation. The effect of temperature on the oxidation performance of carbon composite bricks is more complicated. The oxidation process of carbon composite bricks consists of SiC oxidation weight gain and graphite C oxidation weight loss. In the temperature range of 800–1100 K, the main reaction is the oxidation of C. The oxidation reaction of SiC and the oxidation reaction of graphite C mainly occur at the temperature of 1100–1500 K.

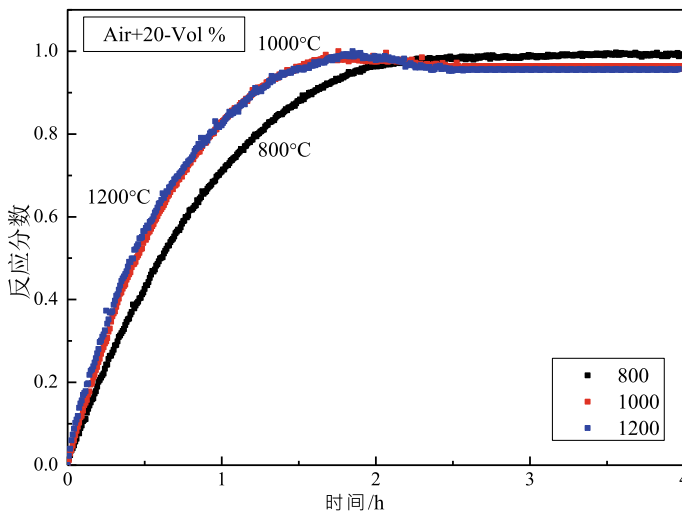


Fig. 6 Oxidation behavior of carbon bricks at different temperatures

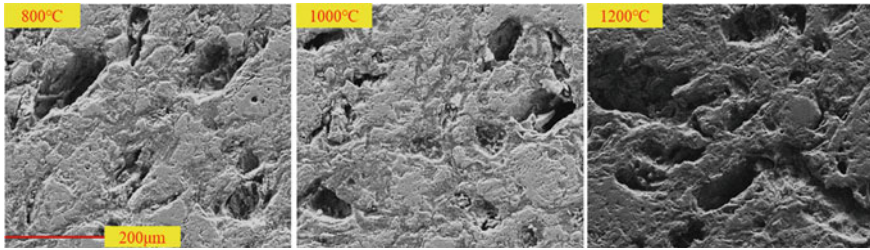


Fig. 7 SEM diagram of carbon composite brick after reaction under wet air condition

Analysis of Erosion Mechanism of Carbon Composite Brick After Service

In the process of damage investigation, it was found that there was obvious slag phase erosion in the taphole area. The location of slag phase erosion is shown in Fig. 8. It is located inside the carbon composite brick on the hot surface of the castable, which is different from the erosion phenomenon of the carbon brick on the hot surface.

According to the difference in macroscopic morphology, the eroded samples can be divided into cyan slag phase erosion area, white-brown slag phase erosion area,

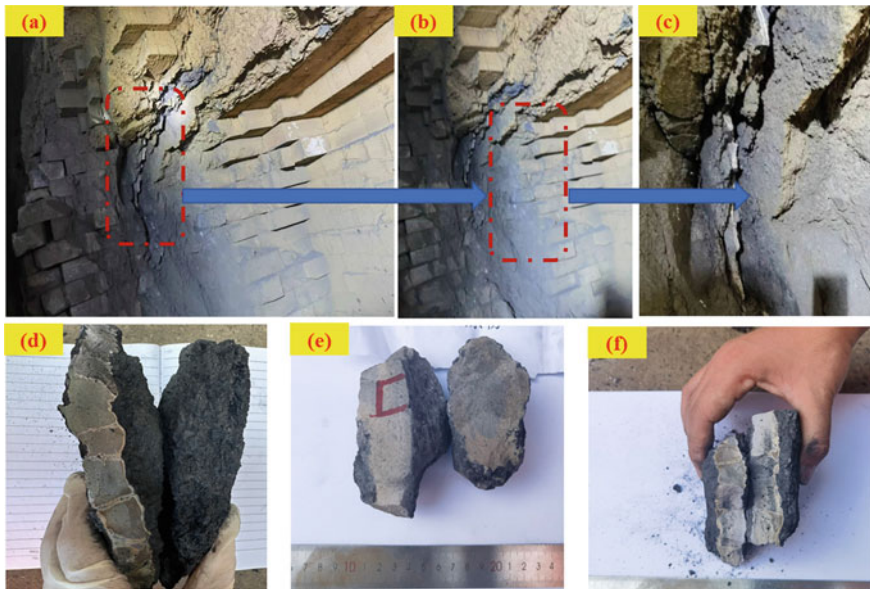


Fig. 8 Macroscopic morphology of slag phase erosion area and sample morphology with (a, b, c) Macroscopic morphology of slag phase erosion area with erosion samples with different morphologies (d Blue-white sample, c Grey-brown sample, Dark-brown sample)

and gray-brown slag phase erosion area. The samples in the non-region were tested by SEM–EDS.

As shown in Fig. 9, the eroded samples of the blue-white slag phase can be divided into three levels according to the degree of erosion, and the elemental composition of different regions is analyzed, respectively. The results are as follows (Table 2).

The area where P1 is located is the area where the carbon composite brick is located after service, and the bright white area in the sample is the Pb erosion enrichment area; the area where P3 is located is a slag phase erosion enrichment area, and the existing phase is similar to the final slag of the blast furnace. P2 is the transition zone between the slag phase and the carbon composite brick, in which there is also ZnO.

As shown in Fig. 10, the erosion area in the gray-brown sample can also be divided into three levels according to the erosion interface. The P1 area is the slag phase enrichment area, and the element content is similar to the P3 area in the blue-white erosion sample. The P2 region of the gray-brown sample is also a ZnO-rich region. Unlike the P3 region in the bluish-white sample, there is no obvious Pb enrichment in the P3 region of the gray-brown sample, and more ZnO appears in it (Table 3).

The dark-brown sample also exhibits the same phase distribution as the above two samples, and the detection results are shown in Fig. 11. The P1-P3 areas are eroded carbon composite bricks, and there is also the enrichment of the ZnO phase. The main phase in the P4 region is similar to that of the blast furnace slag, and there is also a phenomenon of NaO₂ enrichment. A small amount of NaO₂ appears in the P5 region (Table 4).

Table 2 Blue-white sample EDS results in Fig. 9 (atomic%)

Elements	C	Si	O	Al	Mg	Ca	F	Pb	Zn	Mn	Possible phase
P1	46.30	11.79	15.34	4.19				22.39			C, SiO ₂ , Al ₂ O ₃ , PbO
P2		19.00	48.41	8.15	6.48	13.06	1.93		1.73	1.23	SiO ₂ , Al ₂ O ₃ , MgO, CaO, F, ZnO, MnO
P3		19.16	50.76	8.15	4.28	14.13	2.42			1.11	SiO ₂ , Al ₂ O ₃ , MgO, CaO, F, ZnO, MnO

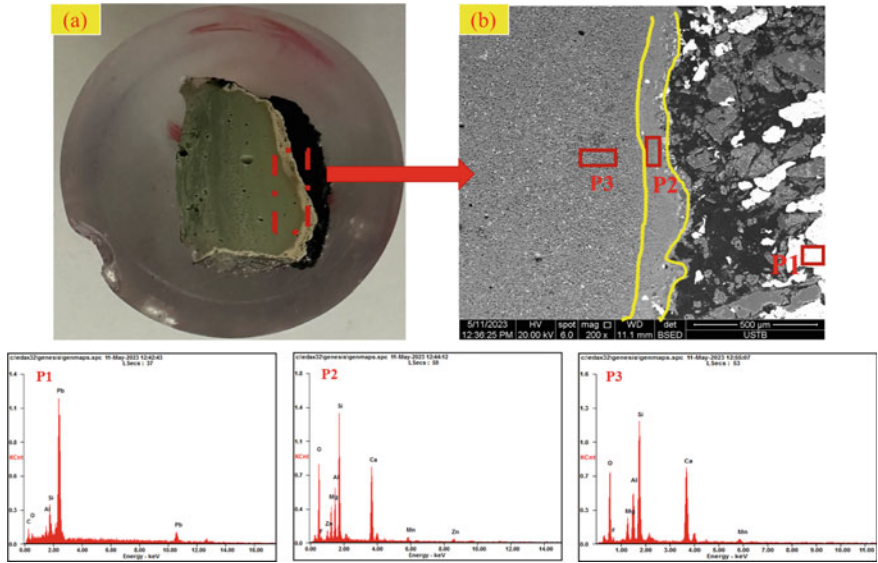


Fig. 9 The macroscopic and microscopic morphology of the blue-white sample with **a** Macroscopic morphology of the blue-white sample and **b** Microstructure of the sample

Table 3 EDS results in Fig. 10 (atomic%)

Elements	C	Si	O	Al	Mg	Ca	F	Pb	Zn	Mn	Possible phase
P1		19.21	51.08	8.33	4.42		2.25			1.20	SiO ₂ , Al ₂ O ₃ , MgO, CaO, F, MnO
P2	12.74	14.11	44.96	5.98	4.66	13.00	1.3		1.76	1.48	C, SiO ₂ , Al ₂ O ₃ , MgO, CaO, F, ZnO, MnO
P3	38.56	2.15	35.35	18.31		1.02			3.99	0.63	C, SiO ₂ , Al ₂ O ₃ , MgO, CaO, ZnO, MnO

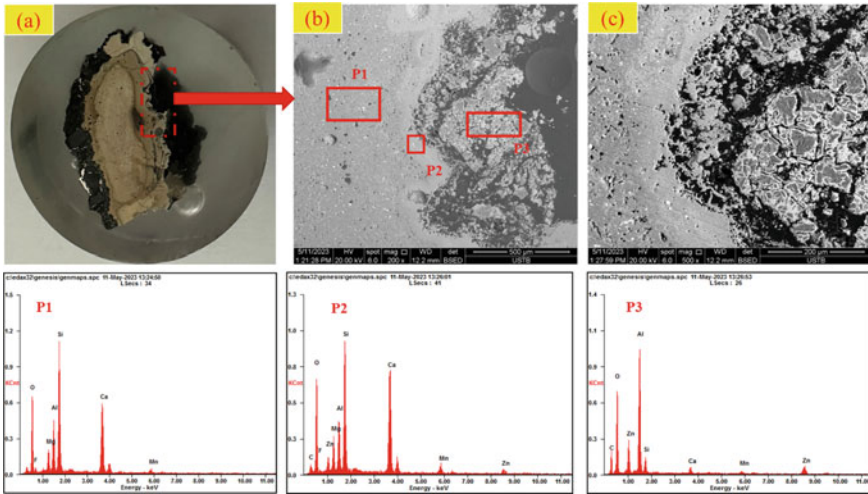


Fig. 10 The macroscopic and microscopic morphology of the gray-brown sample with **a** Macroscopic morphology of the gray-brown sample and **b** Microstructure of the sample

Table 4 EDS results in Fig. 4 (atomic%)

Elements	C	Si	O	Al	Mg	Ca	F	Pb	Zn	Mn	Na	Possible phase
P1	18.40	6.42	43.73	22.62	0.39	2.35			5.12			C, SiO ₂ , Al ₂ O ₃ , MgO, CaO, ZnO
P2	57.04		10.99					25.63	6.35			C, ZnO, PbO,
P3	11.73	17.00	47.79	7.89	4.27	10.72						C, SiO ₂ , Al ₂ O ₃ , MgO, CaO, ZnO
P4		16.50	49.44	6.32	4.92		3.78	0.18		1.05	3.07	SiO ₂ , Al ₂ O ₃ , MgO, CaO, PbO, NaO ₂
P5	13.42	15.85	45.76	7.23	3.61	11.04	1.45			0.68	0.095	SiO ₂ , Al ₂ O ₃ , MgO, CaO, NaO ₂

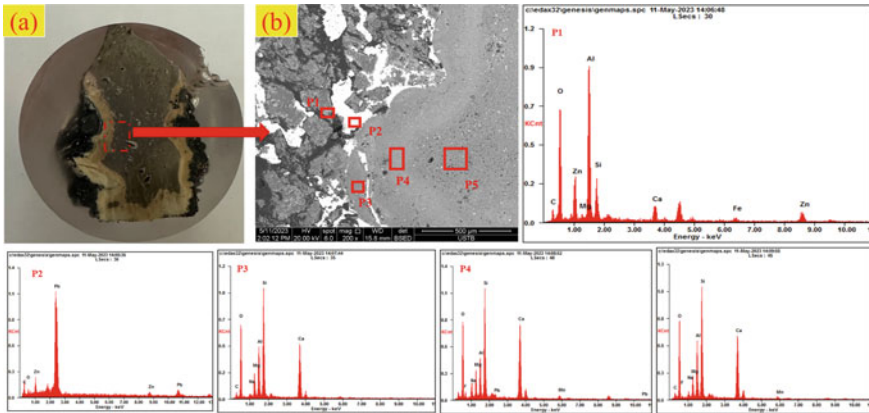


Fig. 11 The macroscopic and microscopic morphology of the dark-brown sample with **a** Macroscopic morphology of the dark-brown sample and **b** Microstructure of the sample

Damage Mechanism Analysis of Hearth Carbon Composite Brick

According to the above detection and experimental results, the phenomenon of slag phase erosion in the blast furnace is analyzed. It is considered that the occurrence of erosion has gone through the following stages.

Water Vapor Oxidation and Carbon Brick Microcrack Generation

In the process of smelting, a hydrogen-rich blast furnace inevitably produces a large amount of water vapor in the tuyere area of the hearth. On the one hand, it reacts with water gas in the dead material column of the hearth, and on the other hand, it diffuses along the refractory of the hearthside wall. According to the results of electron microscope observation, the oxidation reaction of carbon composite bricks occurs under the action of water vapor and oxygen, which leads to the weight loss of carbon bricks and the appearance of cracks.

Erosion of Slag Phase and Harmful Elements

Under the working conditions of steam and hearth temperature changes, the microcracks generated by carbon bricks become the path of slag phase and harmful element erosion. The content of Al_2O_3 and SiO_2 in the carbon composite brick is high, and the slag phase in the blast furnace is more likely to react when in contact with the carbon composite brick. The K and Na in the blast furnace also penetrate the carbon composite brick in the form of steam, and the products are nepheline and garnet.

Formation of Slag Phase Erosion Layer

After the slag phase is eroded into the carbon brick, it continuously reacts with the carbon brick and solidifies in the area where the cold surface temperature is low. Due to the different crystallization temperatures, the samples after the slag phase erosion have slight differences in the macroscopic morphology, and a small amount of Pb erosion occurs in the carbon brick after service. The erosion of water vapor and the fluctuation of hearth temperature lead to the generation of micro-cracks in carbon bricks, and the further erosion of the slag phase and harmful elements leads to the erosion of the slag phase in the hearth area.

Corrosion Resistance Analysis of Carbon Composite Brick Under Actual Production Conditions

Based on the results of the water vapor oxidation experiment and damage investigation, it can be seen that the carbon composite brick will cause a certain degree of structural damage due to the erosion of water vapor at high temperatures. The area of slag phase erosion of carbon composite bricks after service is concentrated in the taphole area, and the structure of carbon composite bricks on the hot and cold surfaces of the eroded area is relatively intact, which is related to the actual production of the blast furnace. Due to the frequent iron tapping in the taphole area, the slag-iron erosion of the refractory in this area is more serious. In this case, once a string of gas appears at the taphole, it will cause further erosion of high-temperature water vapor and alkali metal vapor. Therefore, in actual production, for the taphole area, more attention should be paid to the leakage of cooling equipment to ensure good cooling intensity, which can reduce the erosion of carbon composite bricks to a certain extent.

Conclusions

1. During the damage investigation of a blast furnace injected with hydrogen-rich gas, a slag phase erosion layer with a thickness of 5–15 cm was found in the taphole area.
2. The microscopic morphology observation and composition phase analysis of the samples in the slag phase erosion area were carried out. It was found that there was an obvious interface between the carbon brick and the slag phase after erosion. There was an enrichment of harmful elements such as Zn and Na in the interface transition area. The enrichment of Pb appeared on the carbon brick matrix.
3. Through the experimental study on the resistance of carbon composite bricks to water vapor oxidation, the thermodynamic conditions for the oxidation of carbon composite bricks in a water vapor environment were clarified. The microscopic

morphology observation results after the test showed that the oxidation of water vapor led to micro-cracks and a large number of pores in carbon bricks.

4. The pores and cracks on the surface of the carbon composite brick become the path of slag and harmful element steam. The slag and harmful elements that erode into the carbon composite brick react with the carbon composite brick, and the product forms a macroscopic slag phase erosion phenomenon.
5. The slag phase erosion area is concentrated in the taphole area, and the carbon composite bricks on the cold and hot surfaces of the erosion area are retained in the completed state. The frequent erosion of slag and iron in the Iron Mouth area is the main cause of abnormal erosion in this area. Because of this abnormal erosion phenomenon in hydrogen-rich blast furnaces, the composition of the slag phase can be regulated to promote the formation of a slag-rich protective layer on the hot surface of carbon composite brick. The existence of a slag-rich protective layer can prevent the diffusion of water vapor and alkali metal vapor, and prevent the erosion of carbon composite bricks.

Acknowledgements This work was financially supported by the National Natural Science Foundation of China (No. 52204334).

References

1. Wang XY, Li B, Lu C et al (2022) China's iron and steel industry carbon emissions peak pathways. *Res Environ Sci* 35(2):339
2. Shao YJ, Xu L, Liu XP, Chen HZ (2022) Discussion on the solution of "carbon neutrality" in China's steel production. *China Metall* 32(4):1
3. Xin Y, Cui YK, Tian JL et al (2022) Application status and prospect of low carbon technology in iron and steel industry. *Chin J Eng* 44(4):801
4. Liu ZJ, Zhang JL, Zuo HB, Yang TJ (2012) Recent progress on long service life design of Chinese blast furnace hearth. *ISIJ Int* 52:1713–1723
5. Akihiko S, Hitoshi N, Nariyuki Y et al (2003) Investigation of blast-furnace hearthside wall erosion by core sample analysis and consideration of campaign operation. *ISIJ Int* 43:321–330
6. Zhang FM (2013) Design and operation control for a long campaign life of blast furnaces. *J Iron Steel Res Int* 20:53–60
7. Zhang S, Lee WE (2002) Carbon containing castables: current status and prospects. *Br Ceram Trans* 101:1–8
8. Prompt N, Ouedraogo E (2008) High-temperature mechanical characterization of an alumina refractory concrete for blast furnace main trough: Part I. General context. *J Eur Ceram Soc* 28:2859–2865
9. Luz AP, Miglioli MM, Souza TM et al (2012) Effect of Al_4SiC_4 on the Al_2O_3 -SiC-SiO₂-C refractory castables performance. *Ceram Int* 38:3791–3800
10. Zuo HB, Wang C, Zhang JL, Zhao YA, Jiao KX (2015) Oxidation behavior and kinetics of Al_2O_3 -SiC-SiO₂-C composite in air. *Ceram Int* 41:9093–9100
11. Zuo HB, Wang C, Liu YL (2017) Dissolution behavior of a novel Al_2O_3 -SiC-SiO₂-C composite refractory in blast furnace slag. *Ceram Int* 43:7080–7087
12. Zhou Y (1998) Analysis and countermeasures of "garlic like" erosion on blast furnace hearth. *Iron and Steel* 33(2):4–6

13. Cheng K, Jorg M (2006) Factors affecting the service life of carbon bricks at the bottom and hearth of blast furnace. *Ironmaking* 25(1):11–15
14. Xiao Y (2002) Damage of refractory materials for blast furnace. *Refractor Lime* 2:7–10
15. Luo M, Li Y, Jin S et al (2013) Microstructure and mechanical properties of multi-walled carbon nanotubes containing Al_2O_3 -C refractories with addition of polycarbosilane. *Ceram Int* 39(5):4831–4838
16. Wang Q, Li Y, Luo M et al (2014) Strengthening mechanism of grapheme oxide nanosheets for Al_2O_3 -C refractories. *Ceram Int* 40(1):163–172
17. Liu Y, Zhang J, Hou X et al (2015) Oxidation behavior of carbon bricks for blast furnace hearth under high temperature and water content. *Min Metall* 24(S1):75–81